Silicon (2022) 14:11503–11517
https://doi.org/10.1007/s12633-022-01884-4

ORIGINAL PAPER

Prediction of Element Transfer Behaviour in SAW Process Using SiO_2-CaO-TiO_2 & Al_2O_3-SiO_2-CaO Silica Based Flux Systems

Lochan Sharma[1] · Rahul Chhibber[2] · Aditya Kumar[2] · Deepak Bhandari[3]

Received: 7 February 2022 / Accepted: 6 April 2022 / Published online: 13 April 2022

Abstract

Weld mechanical as well as metallurgical properties are widely affected by the flux composition. Selection of flux composition play an important role in determining the good bead quality and mechanical properties of the welded joint. By using laboratory developed agglomerated rutile basic fluxes a study has been carried out to predict the element transfer behaviour in submerged arc welding process (SAW). With the application of mathematical experiments of mixture design approach different statistical model were developed in terms of flux constituents. Using twenty one rutile basic submerged arc welding fluxes a series of bead on plate weld deposits were made at constant welding parameters. Twenty one submerged arc welding fluxes were prepared as per mixture design approach for SiO_2-CaO-TiO_2 & Al_2O_3-SiO_2-CaO flux system. Regression models were developed in terms of individual, binary and ternary mixture flux constituents for different Δ quantities. Mathematical regression models have been checked for 95% significance level by using F-test. Results indicates that there was predominant effect on weld metal carbon, silicon, manganese, sulphur, phosphorous, molybdenum and chromium contents. Individual flux ingredients CaO and SiO_2, has synergistic effect on Δ_C and increases its weld bead carbon content while TiO_2 and Al_2O_3 shows antisynergistic effect on Δ_C and decreases the delta carbon content in weld region.

Keywords API X70 steel · Flux composition · SAW · Delta quantities · Mixture design approach

1 Introduction

The pipeline grade most commonly used evolved rapidly from X52 to X60 and then X65 to X70 in 1990. In 1993, a new grade X80 to the pipeline family came with parallel development in X70. The need for the development of X70 and X80 grade was that an alloy system used for X65 production consisting of titanium stabilized carbon manganese steel strengthened with niobium and vanadium which had a limited ability to be extended to higher strengths. Carbon equivalent (CE) approaches to an unacceptable level as strength increases due to the addition of higher alloy constituents. Carbon equivalent plays an important role in deciding the weldability of high strength low alloy pipeline steels. Crack sensitivity of high strength low alloy pipeline steels were well decided by carbon equivalent value. Higher value (CE > 0.45) of carbon equivalent means HSLA steels are more prone to failure due to poor weldability. For this reason, vanadium was replaced by molybdenum, a strong carbide former and the very effective strengthening agent was added in X70 steel. The high effectiveness of molybdenum along with the use of niobium allows the formation of a strong alloy which made X70 steel more suitable in severe service environment. The most economic and safe way of transport for oil and gas is pipeline, steel such as API X70, X80, X100 etc. are widely acceptable as pipeline steel [1]. Superior manufacturing process

✉ Lochan Sharma
lochan.e9455@cumail.in

Rahul Chhibber
rahul_chhibber@iitj.ac.in

Aditya Kumar
kumar.141@iitj.ac.in

Deepak Bhandari
bhnadari2k@rediffmail.com

[1] University Centre of Research and Development, Chandigarh University, Gharuan, Punjab, India

[2] IIT Jodhpur, Jodhpur, Rajasthan 342011, India

[3] YCOE, Talwandi Saboo, Bathinda, Punjab, India

producing higher grade steel requires more suitable welding process and consumable to match the minimum requirement before installation. This continuous development of pipeline steels along with welding methods enables the pipeline to work with maximum operating pressure. High pressure pipelines are usually joined with submerged arc welding process (SAW) known as seam welding. SAW process requires flux which interacts with the molten and governs the weld metal chemistry [2–4]. Pipeline steels are exposed to the detrimental and corrosive environment which reduces its service life and sometimes leads to pipeline failure. Weld properties such as microstructure, tensile strength and impact toughness hence becomes an important parameter for pipeline weld, these parameters are dependent on the element present in the weld pool. Using suitable welding consumable such welding flux and wire combination weld properties can be improved. This research work is done to develop SAW fluxes for API X70 steel and to study the individual and interaction effect of flux constituents on element transfer behaviour. Due to tremendous inherent features such as smooth finish, high quality, deep penetration and joining of thicker sections submerged arc welding process is frequently utilized in the pipeline industry. In submerged arc welding process, flux mixture disintegrated in arc column while at same time filler wire melted and transferred into the weld region resulting in the formation slag which prevents the molten weld region from atmospheric environment. Due to metallurgical reactions, there are some chances of loss of filler metal by oxidation or evaporation while some of the flux constituents may possible to enter in the weld pool region. Final weld metal composition is mainly decided by how well metal transfer takes place during submerged arc welding process. Physicochemical and thermophysical properties of submerged arc fluxes widely affected by cooling rate, slag behaviour and final weld joint properties such as tensile strength, impact toughness etc. during submerged arc welding. Submerged arc welding utilizes gravity fed flux to blanket the arc, this setup results in high thermal arc efficiency. Due to covered arc SAW process is capable of using higher heat input which leads to higher metal deposition rate, suitable for joining thick pipeline sections. Fluxes used for SAW enhances arc stability, reduces heat loss, improves surface cleanliness, reduces spatter etc. Slag metal reaction within the weld pool takes place which converts flux into slag which floats and gets deposited over the weld, during this reaction various elements gets transfer to the weld depending upon the reactivity of the flux. During SAW welding there are various parameters that affect the of weld such voltage, current, polarity, flux composition, welding speed etc. these parameters interact in the weld pool giving reactions between steel and slag which governs the chemical and physical properties of the weldment [5–7]. Weld zone being a nonhomogeneous part to the weldment has different chemistry which can be controlled by the varying previously mentioned parameter and weld wire composition. Research work on metallurgical changes on weld with the slag metal reaction can help to regulate the metal chemistry. Flux composition governs the slag behaviour while reacting with molten steel hence deciding the element transfer to the weld pool [8, 9]. Flux should contain a proper thermophysical and physicochemical properties to yield the desired the welding metal chemistry [10]. Weld metal oxygen and hydrogen should be maintained low which can be controlled by Basicity index of the flux [11]. Prediction of the weld metal chemistry from the flux composition mathematical modelling are found suitable in this regard [12]. In previous study researcher has developed the model to predict the element transfer behaviour with flux compositions and compared with empirical model to predict oxygen ppm [13]. Weld chemistry is greatly influenced by the binary interaction of parameters including flux rather than individual effect of flux constituents, polarity was found as an important parameter. In previous literature influence of flux constituents were studied on the transfer of element such as oxygen, manganese, silica, sulphur and carbon. It was concluded that Mn percentage in the weld metal is dependent on the electrochemical reaction taking in weld pool, whereas silica transfer was resulted due to electrochemical reaction and thermochemical dissociation in molten weld pool [14–16]. Available literature suggests that only the thermodynamic data is not sufficient for the prediction of slag metal reaction in weld pool, this study evaluated the weld metal chemistry with the addition of CaF_2, CaO, and FeO on flux [17]. In previous study the effect of Ti (0.01–0.08%) and Mn (1.4–2%) micro alloy addition at different weight percentage on API 5 L-X70 steel was observed. Excellent mechanical behavior in the weld series was achieved in two configurations, i.e. 1.92% Mn-0.02% Ti and 1.40% Mn-0.08% Ti. With the addition of titanium in the range of 0.02–0.08%, acicular ferrite phase was developed in the microstructure which gives good mechanical properties of weld metal [18]. The influence of Ni content (0.50 wt.% - 3.11 wt.%) on the impact toughness and microstructure of C-Mn weld metal was observed during submerged arc welding. Ni amount up to 1 wt.% enhances the weld metal impact toughness due to gain in acicular ferrite content and microstructural refinement. Weld toughness reduced due to the formation of martensite-austenite (M-A) constituent at higher nickel content [19]. Y. Yoshino et al. studied the effect of niobium weight percentage (0.01–0.04 wt.%) on weld metal to improve low-temperature notch toughness and its strength. It was observed that higher weight percentage of niobium (>0.03%) in the weld region significantly reduces its impact toughness due to precipitation of niobium carbo-nitrides. Up to 65% of niobium pick up in the weld produced during submerged arc welding even with niobium free filler materials. The volume of proeutectoid ferrite reduced and that of acicular ferrite enlarged with the incorporation of niobium. In submerged arc welding notch toughness greatly affected by the interaction of niobium with other alloying elements [20]. This paper presents an experimental study of the role of welding flux constituents and their interactions on the delta (Δ) element transfer during SAW process.

2 Experimentation

2.1 Design of Flux Matrix

In present work the composition of rutile basic fluxes, based on SiO_2-CaO-TiO_2 & Al_2O_3-SiO_2-CaO flux systems was developed with the help of constrained mixture design shown in Table 1 [21]. By changing the composition of 4 rutile basic flux constituents Al_2O_3, TiO_2, SiO_2 and CaO and keeping the bentonite content fixed these fluxes were prepared. A total of 21 fluxes were developed with varying compositions. These fluxes interact and dissociates with flux wall guided of type of metal transfer in the weld pool. To decide the suitable range of fluxes two ternary phase diagrams were used as shown in Fig. 1a-b. Minimum and maximum range of flux constituents is shown by Eq. 1 with total maximum constraint is 90%.

$$\begin{aligned} 15.9 \le & \mathrm{CaO}\ (t_1) \le 32 \\ 24 \le & \mathrm{TiO_2}\ (t_2) \le 37 \\ 10 \le & \mathrm{SiO_2}\ (t_3) \le 27 \\ 7 \le & \mathrm{Al_2O_3}\ (t_4) \le 12 \\ & \sum_{i=1}^{4} t_i = 90 \end{aligned} \tag{1}$$

Table 1 Design of flux matrix

Exp. Runs	F_{RB}	Points	Flux elements			
			CaO	TiO_2	SiO_2	Al_2O_3
1.	F_1	V	32.0	30.0	20.9	7.0
2.	F_2	V	20.1	34.3	23.5	12
3.	F_3	V	30.1	24.0	27.0	8.8
4.	F_4	V	28.9	37.0	16.5	7.4
5.	F_5	V	28.9	37.0	16.5	7.4
6.	F_6	V	32.0	25.2	20.7	12.0
7.	F_7	EC	32.0	30.0	20.9	7.0
8.	F_8	EC	26.5	31.8	21.8	9.6
9.	F_9	EC	26.8	29.1	27.0	7.0
10.	F_{10}	EC	21.6	29.3	27.0	12.0
11.	F_{11}	EC	27.5	37.0	13.4	12.0
12.	F_{12}	EC	22.4	37.0	18.5	12.0
13.	F_{13}	EC	26.8	26.7	24.3	12.0
14.	F_{14}	EC	32.0	36.4	10.0	11.5
15.	F_{15}	PC	15.9	37.0	27.0	10.0
16.	F_{16}	PC	27.8	32.5	19.3	10.2
17.	F_{17}	PC	32.0	31.0	14.9	12.0
18.	F_{18}	PC	22.6	33.4	26.8	7.0
19.	F_{19}	PC	26.5	31.8	21.8	9.6
20.	F_{20}	PC	26.5	31.8	21.8	9.6
21.	F_{21}	OC	26.5	31.8	21.8	9.6

V Vertex, *EC* Edge centre, *PC* Plane centre, *OC* Overall centre

2.2 Element Transfer Evaluation

Bead on plate were laid with the granulated flux using SAW process and chemical analysis was carried out and its composition shown in Table 2. Increment or the decrement of the flux elements from slag to weld and vice versa was shown as the 'Δ' delta of the flux element. To observe the element transfer due to flux a delta quantity (Δ) was used which is obtained by the difference of expected and observed weld metal content. Equation 2 is used to evaluate the dilution (D) due to parent metal as well due to filler wire (1-D) in submerged arc welding process. Equation 3 was used to find the expected weld metal dilution content. Table 3 represents the dilution values and chemical composition of weld bead deposits while Table 4 represents the observed as well as (Δ) transfer quantities by flux.

$$\text{Dilution (D)} = \text{Parent metal Area}/\text{Parent mental area} + \text{Fused area of filler wire} \tag{2}$$

$$\text{Expected weld content} = \text{D x Parent metal element content} + (1-\text{D})\ \text{Filler wire element content} \tag{3}$$

3 Results & Discussion

Regression analysis is used to model the flux constituents and their responses i.e. weld bead chemistry and further multiresponse optimization is used to validate the results.

3.1 Development of Regression Models

Least square regression equations (Eqs. 4–11) in terms of percentage composition of flux constituents were formed by using observed values of chemical composition from experimentation. Second and third order regression models were formed in terms of primary, secondary & ternary flux mixture interactions. ANOVA has been used to check the adequacy of the predicted equations. By finding the F and P values at 95% confidence level the whole mixture models has been verified for linear, quadratic and cubic square models [23]. In order to find the significance and accuracy of regression models analysis of variance (ANOVA) of different delta quantities were evaluated. F value measures the variation of the data about its mean value. F values less than 0.05 indicates that model terms are significant. Values greater than 0.1 indicate the model terms are not significant. The model's goodness of fit can validate with the help of

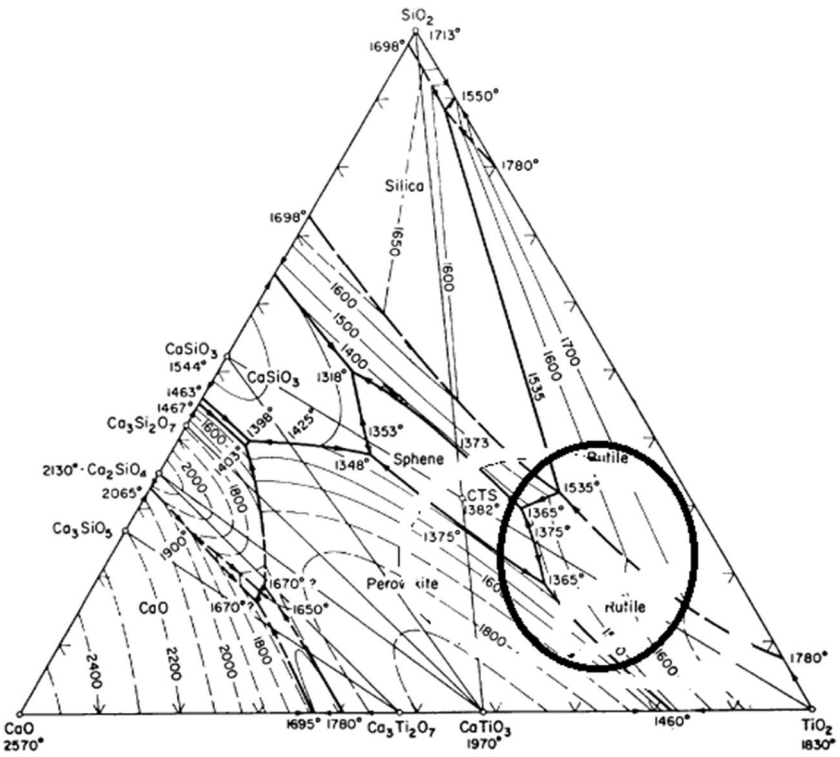

(a)

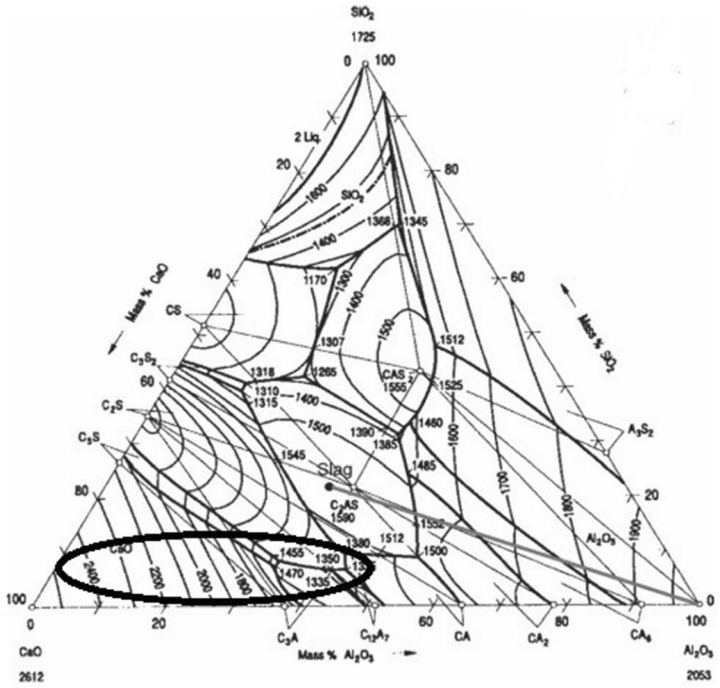

(b)

Fig. 1 **a**-**b** Ternary Phase diagrams [9, 22]

Table 2 Chemical composition of base metal and filler wire

Material	*C*	*Si*	*Mn*	*P*	*S*	*Mo*	*Ni*	*Cr*	*Fe*
PM (X70)	0.063	0.321	1.640	0.007	0.001	0.001	0.318	0.006	97.5
FW (EA2TiB)	0.029	0.088	0.871	0.010	0.007	0.216	0.084	0.032	98.4

Table 3 Dilution values and chemical composition of weld bead

			Expected weld bead content (%)								
Flux	*D*	*D-1*	*C*	*Si*	*P*	*S*	*Mn*	*Ni*	*Cr*	*Mo*	*CE*
f1	0.45	0.55	0.0559	0.3654	0.0244	0.0039	0.8518	0.0073	0.0646	0.3029	0.26
f2	0.48	0.52	0.0503	0.3432	0.0146	0.0021	0.5634	0.0079	0.0630	0.2809	0.21
f3	0.34	0.66	0.0456	0.5022	0.0152	0.0024	0.6178	0.0081	0.0664	0.2657	0.21
f4	0.39	0.61	0.0403	0.5979	0.0149	0.0023	0.3955	0.0085	0.0494	0.3448	0.19
f5	0.36	0.64	0.0454	0.4404	0.0145	0.0017	0.4966	0.0080	0.0617	0.2985	0.20
f6	0.30	0.70	0.0501	0.3631	0.0157	0.0021	0.4526	0.0087	0.0571	0.3094	0.20
f7	0.40	0.60	0.0499	0.2899	0.0166	0.0020	0.5461	0.0079	0.0678	0.2816	0.21
f8	0.37	0.63	0.0498	0.3029	0.0176	0.0051	0.5220	0.0083	0.0575	0.2840	0.21
f9	0.32	0.68	0.0496	0.3289	0.0185	0.0039	0.5012	0.0090	0.0639	0.3041	0.21
f10	0.31	0.69	0.0451	0.4752	0.0175	0.0029	0.4584	0.0084	0.0594	0.3113	0.20
f11	0.36	0.64	0.0483	0.4269	0.0159	0.0023	0.4262	0.0089	0.0556	0.3387	0.20
f12	0.37	0.63	0.0519	0.3656	0.0166	0.0024	0.4873	0.0089	0.0603	0.3065	0.21
f13	0.31	0.69	0.0530	0.3247	0.0248	0.0041	0.4476	0.0086	0.0678	0.3033	0.20
f14	0.27	0.73	0.0572	0.3077	0.0217	0.0035	0.6346	0.0076	0.0771	0.2510	0.24
f15	0.32	0.68	0.0521	0.4296	0.0263	0.0045	0.3889	0.0074	0.0621	0.3117	0.19
f16	0.40	0.60	0.0514	0.4273	0.0261	0.0051	0.3463	0.0073	0.0577	0.3210	0.19
f17	0.33	0.67	0.0549	0.3348	0.0273	0.0049	0.3637	0.0071	0.0628	0.3132	0.19
f18	0.36	0.66	0.0468	0.5528	0.0242	0.0057	0.3589	0.0079	0.0540	0.3469	0.19
f19	0.29	0.71	0.0543	0.3818	0.0233	0.0047	0.4695	0.0072	0.0627	0.3028	0.21
f20	0.41	0.59	0.0527	0.5249	0.0252	0.0047	0.4078	0.0075	0.0604	0.3186	0.20
f21	0.28	0.72	0.0522	0.5377	0.0215	0.0050	0.4671	0.0075	0.0615	0.2683	0.20

Table 4 Observed values as well as (Δ) transfer quantities by flux

Flux	Δ*C*	Δ*Si*	Δ*Mn*	Δ*P*	Δ*S*	Δ*Mo*	Δ*Ni*	Δ*Cr*
f1	0.0116	0.17255	−0.36525	0.01575	−0.0004	0.18365	−0.182	0.0443
f2	0.00498	0.14336	−0.67672	0.00604	−0.00202	0.1681	−0.18842	0.04348
f3	0.00504	0.33498	−0.51466	0.00622	−0.00256	0.1228	−0.15546	0.04324
f4	−0.00196	0.41903	−0.77541	0.00607	−0.00236	0.21265	−0.16676	0.02754
f5	0.00416	0.26852	−0.65124	0.00558	−0.00314	0.1599	−0.16024	0.03906
f6	0.0109	0.2052	−0.6491	0.0066	−0.0031	0.1579	−0.1455	0.0329
f7	0.0073	0.1087	−0.6325	0.0078	−0.0026	0.1516	−0.1697	0.0462
f8	0.00822	0.12869	−0.63353	0.00871	0.00032	0.14755	−0.16228	0.03512
f9	0.00972	0.16634	−0.61588	0.00946	−0.00118	0.1569	−0.14988	0.04022
f10	0.00556	0.31497	−0.65099	0.00843	−0.00224	0.16195	−0.14814	0.03546
f11	0.00706	0.25502	−0.72164	0.00698	−0.00254	0.2001	−0.15934	0.03296
f12	0.01032	0.19139	−0.66823	0.00771	−0.00238	0.17005	−0.16168	0.03792
f13	0.01346	0.16447	−0.66179	0.01573	−0.00104	0.15395	−0.14794	0.04386
f14	0.01902	0.15679	−0.44403	0.01251	−0.00188	0.09305	−0.13958	0.05212
f15	0.01222	0.26704	−0.72818	0.01726	−0.00058	0.1645	−0.15148	0.03842
f16	0.0088	0.2461	−0.8323	0.0173	0.0005	0.1910	−0.1703	0.0361
f17	0.01468	0.16991	−0.76107	0.01829	−0.00012	0.16815	−0.15412	0.03938
f18	0.00556	0.38092	−0.78894	0.01528	0.00086	0.2083	−0.16034	0.03136
f19	0.01544	0.22623	−0.62451	0.01417	−0.00056	0.14915	−0.14466	0.03824
f20	0.00976	0.34137	−0.77849	0.01643	0.00016	0.19075	−0.17244	0.03906
f21	0.01368	0.38446	−0.61922	0.01234	−0.00032	0.1125	−0.14202	0.03678

determination regression coefficient (R^2). The closer the R^2 value is to 1, the better the correlation between the **experimental** and **predicted** values is. A prediction plot shows the actual targets from the dataset against the predicted values generated by our model. This allows us to see how much variance is in the model. Figure 2a-b represents the predicted vs. actual values for all the responses. For a good fit, the dataset points should be close to fitted line. From Fig. 2a-b it has been clearly observed that the data points for Δ_P, Δ_S and Δ_{Cr} are close to the fitted line as compared to the remaining delta responses. Table 5 represents the ANOVA results with R^2 values for all the responses.

$$\begin{aligned}\Delta C = {} & +0.001119.CaO-0.004694.TiO_2 \\ & + 0.000541.SiO_2-0.031334.Al_2O_3 \\ & + 0.000044.CaO.TiO_2-0.000076.CaO.SiO_2 \\ & + 0.000431.CaO.Al_2O_3 + 0.000104.TiO_2.SiO_2 \\ & + 0.000590.TiO_2.Al_2O_3 + 0.000299.SiO_2.Al_2O_3 \end{aligned} \quad (4)$$

$$\begin{aligned}\Delta Si = {} & -0.067363.CaO + 0.081168.TiO_2 \\ & + 0.027183.SiO_2-0.591090.Al_2O_3 \\ & -0.000268.CaO.TiO_2 \\ & +0.000679.CaO.SiO_2 \\ & + 0.011802.CaO.Al_2O_3-0.002132.TiO_2.SiO_2 \\ & + 0.003976.TiO_2.Al_2O_3 + 0.008975.SiO_2.Al_2O_3 \end{aligned} \quad (5)$$

$$\begin{aligned}\Delta Mn = {} & +0.093348.CaO-0.037747.TiO_2 \\ & + 0.075761.SiO_2-0.177097.Al_2O_3 \\ & -0.000771.CaO.TiO_2-0.002384.CaO.SiO_2 \\ & -0.003571.CaO.Al_2O_3-0.001846.TiO_2.SiO_2 \\ & + 0.006081.TiO_2.Al_2O_3 \\ & + 0.002091.SiO_2.Al_2O_3 \end{aligned} \quad (6)$$

$$\begin{aligned}\Delta P = {} & +0.090189.CaO-0.019883.TiO_2 \\ & + 0.163063.SiO_2 \\ & + 0.348135.Al_2O_3-0.000332\ CaO.TiO_2 \\ & -0.005977.CaO.SiO_2-0.012886.CaO.Al_2O_3 \\ & -0.001734.TiO_2.SiO_2-0.003847.TiO_2.Al_2O_3 \\ & -0.019077.SiO_2.Al_2O_3 \\ & + 1.61265E-07.CaO.TiO_2.SiO_2 \\ & + 0.000073.CaO.TiO_2.Al_2O_3 \\ & + 0.000525.CaO.SiO_2.Al_2O_3 \\ & + 0.000187.TiO_2.SiO_2.Al_2O_3 \end{aligned} \quad (7)$$

$$\begin{aligned}\Delta S = {} & -0.000995.CaO-0.001843.TiO_2-0.000554.SiO_2 \\ & -0.011501.Al_2O_3 + 0.000044.CaO.TiO_2 \\ & + 1.96798E-06.CaO.SiO_2 \\ & + 0.000192.CaO.Al_2O_3 + 0.000054.TiO_2.SiO_2 \\ & + 0.000188.TiO_2.Al_2O_3 + 0.000120.SiO_2.Al_2O_3 \end{aligned} \quad (8)$$

$$\begin{aligned}\Delta Mo = {} & -0.009566.CaO \\ & + 0.013632.TiO_2-0.020760.SiO_2 \\ & + 0.323689.Al_2O_3 + 0.000011.CaO.TiO_2 \\ & + 0.000682.CaO.SiO_2-0.003705.CaO.Al_2O_3 \\ & + 0.000461.TiO_2.SiO_2-0.005082.TiO_2.Al_2O_3 \\ & -0.004283.SiO_2.Al_2O_3 \end{aligned} \quad (9)$$

$$\begin{aligned}\Delta Ni = {} & -0.007818.CaO + 0.002715.TiO_2 \\ & + 0.009684.SiO_2-0.065184.Al_2O_3 \\ & + 7.63353E-06.CaO.TiO_2-0.000170.CaO.SiO_2 \\ & + 0.001404.CaO.Al_2O_3-0.000269.TiO_2.SiO_2 \\ & + 0.000503.TiO_2.Al_2O_3 \\ & + 0.000686.SiO_2.Al_2O_3 \end{aligned} \quad (10)$$

$$\begin{aligned}\Delta Cr = {} & -0.028102.CaO-0.113092.TiO_2 + 0.045714.SiO_2 \\ & + 0.029655.Al_2O_3 + 0.004315.CaO.TiO_2. \\ & -0.001479.CaO.SiO_2-0.001287.CaO.Al_2O_3 \\ & + 0.002454.TiO_2.SiO_2 + 0.006990.TiO_2.Al_2O_3 \\ & -0.008847.SiO_2.Al_2O_3-0.000073.CaO.TiO_2.SiO_2 \\ & -0.000222.CaO.TiO_2.Al_2O_3 + 0.000356.CaO.SiO_2.Al_2O_3 \\ & -0.000028.TiO_2.SiO_2.Al_2O_3 \end{aligned} \quad (11)$$

3.2 Influence of Rutile Basic Flux Elements on Different Δ Quantities

The expected weld bead carbon content for all the experiments have been increased (Table 3) but it is lesser than that of parent metal (Table 2). From regression Eq. 4 it has been observed that individual flux ingredients CaO and SiO_2, has synergistic effect on Δ_C and increases its weld bead carbon content while TiO_2 and Al_2O_3 shows antisynergistic effect on Δ_C and decreases the delta carbon content in weld region. All the binary mixture interactions gives synergistic effect on Δ_C and increases its weld metal carbon content except $CaO.SiO_2$ interaction which decreases its weld metal carbon. The increase of weld bead carbon content (Table 3) may be due to reduction of

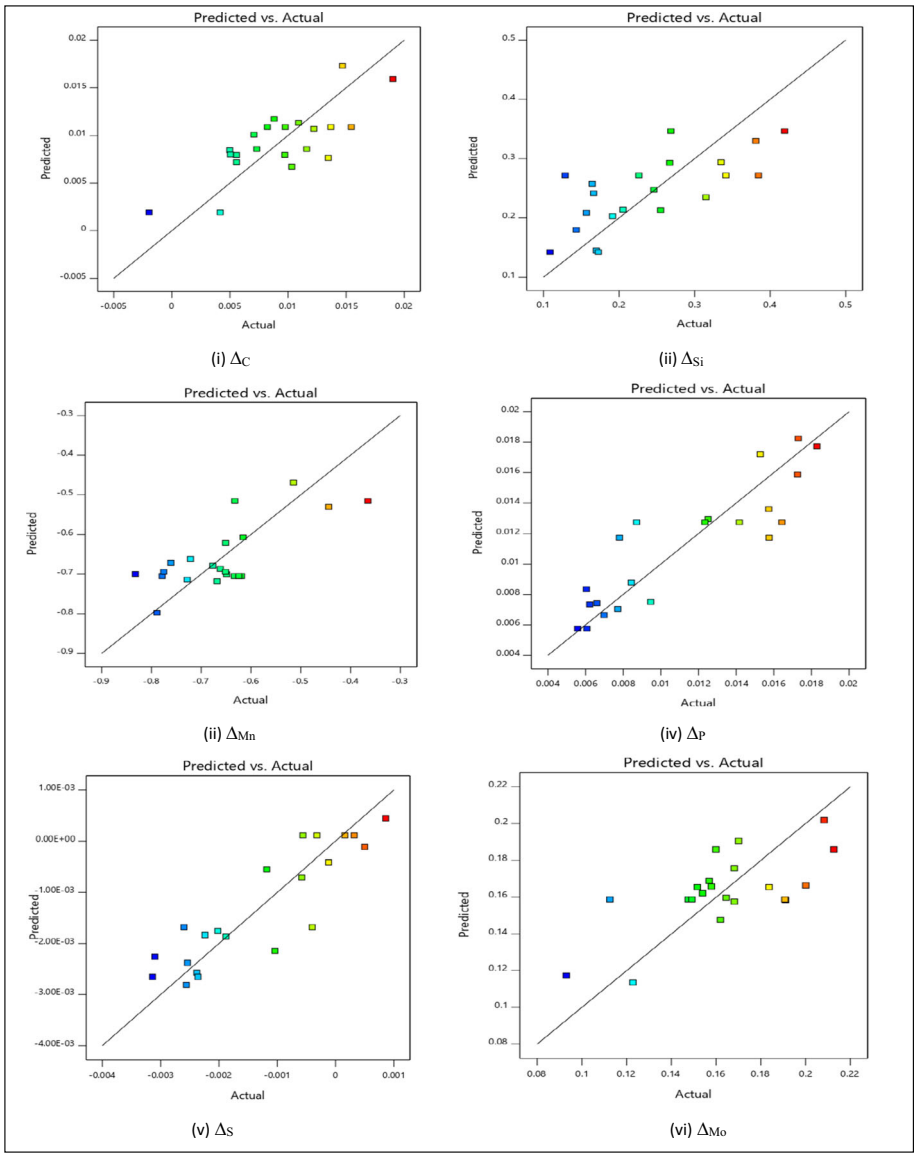

Fig. 2 **a**-**b** Predicted vs. actual plots of Δquantities

Table 5 ANOVA results

Properties	Source	SS	DOF	MSS	F value	P value	R^2 value	Significant
Δ_C	Model	0.0003	9	0.0000	1.73	0.0439	0.75	Significant
	Linear	0.0001	3	0.0000	1.72	0.0195		
	$CaO.TiO_2$	7.061E-06	1	7.061E-06	0.4225	0.0290		
	$CaO.SiO_2$	0.0000	1	0.0000	1.79	0.2078		
	$CaO.Al_2O_3$	0.0001	1	0.0000	1.62	0.2293		
	$TiO_2.SiO_2$	0.0000	1	0.0000	2.65	0.1320		
	$TiO_2.Al_2O_3$	0.0000	1	0.0000	2.67	0.1308		
	$SiO_2.Al_2O_3$	0.0000	1	0.0000	0.7511	0.4046		
	Residual	0.0002	11	0.0000				
	Total	0.0004	20					
Δ_{Si}	Model	0.1129	13	0.0087	0.9957	0.0500	0.80	Significant
	Linear	0.0195	3	0.0065	0.7446	0.0587		
	$CaO.TiO_2$	0.0021	1	0.0021	0.2358	0.0421		
	$CaO.SiO_2$	0.0010	1	0.0010	0.1100	0.0498		
	$CaO.Al_2O_3$	0.0004	1	0.0004	0.0410	0.8454		
	$TiO_2.SiO_2$	0.0002	1	0.0002	0.0249	0.8791		
	$TiO_2.Al_2O_3$	0.0001	1	0.0001	0.0060	0.9406		
	$SiO_2.Al_2O_3$	0.0001	1	0.0001	0.0155	0.9045		
	$CaO.TiO_2.SiO_2$	0.0096	1	0.0096	1.10	0.3296		
	$CaO.TiO_2.Al_2O_3$	0.0061	1	0.0061	0.7044	0.4290		
	$TiO_2.SiO_2.Al_2O_3$	0.0013	1	0.0013	0.1482	0.7117		
	Residual	0.0005	1	0.0005				
	Total		20					
Δ_{Mn}	Model	0.11	9	0.0154	3.48	0.0255	0.86	Significant
	Linear	0.024	3	0.0147	1.41	0.0914		
	$CaO.TiO_2$	0.013	1	0.0021	0.2049	0.0596		
	$CaO.SiO_2$	0.080	1	0.0298	2.86	0.0191		
	$CaO.Al_2O_3$	0.037	1	0.0019	0.1779	0.0813		
	$TiO_2.SiO_2$	0.053	1	0.0140	1.35	0.0704		
	$TiO_2.Al_2O_3$	0.093	1	0.0047	0.4538	0.0144		
	$SiO_2.Al_2O_3$	0.068	1	0.0006	0.0589	0.0128		
	Residual	0.048	11	0.0104				
	Total	0.2537	20					
Δ_P	Model	0.0003	13	0.0000	4.00	0.0116	0.96	Significant
	Linear	3.908E-06	3	1.303E-06	0.1047	0.0547		
	$CaO.TiO_2$	0.0001	1	0.0001	5.56	0.0505		
	$CaO.SiO_2$	0.0000	1	0.0000	2.58	0.0523		
	$CaO.Al_2O_3$	0.0000	1	0.0000	3.68	0.0966		
	$TiO_2.SiO_2$	0.0001	1	0.0001	5.37	0.0537		
	$TiO_2.Al_2O_3$	0.0000	1	0.0000	3.53	0.0024		
	$SiO_2.Al_2O_3$	0.0000	1	0.0000	2.38	0.0670		
	$CaO.TiO_2.SiO_2$	3.020E-10	1	3.020E-10	0.0000	0.0962		
	$CaO.TiO_2.Al_2O_3$	5.849E-06	1	5.849E-06	0.4703	0.0149		
	$TiO_2.SiO_2.Al_2O_3$	0.0000	1	0.0000	2.70	0.0446		
	$TiO_2.SiO_2.Al_2O_3$	0.0000	1	0.0000	3.33	0.0109		
	Residual	0.0001	7	0.0000				
	Total		20					
Δ_S	Model	0.0000	9	2.845E-06	4.58	0.0104	0.98	Significant
	Linear	2.627E-06	3	8.757E-07	1.41	0.2921		
	$CaO.TiO_2$	6.942E-06	1	6.942E-06	11.17	0.0066		

Table 5 (continued)

Properties	Source	SS	DOF	MSS	F value	P value	R^2 value	Significant
	$CaO.SiO_2$	2.030E-08	1	2.030E-08	0.0327	0.8598		
	$CaO.Al_2O_3$	5.357E-06	1	5.357E-06	8.62	0.0135		
	$TiO_2.SiO_2$	0.0000	1	0.0000	19.23	0.0011		
	$TiO_2.Al_2O_3$	4.529E-06	1	4.529E-06				
	$SiO_2.Al_2O_3$	2.024E-06	1	2.024E-06				
	Residual	6.834E-06	11	6.212E-07				
	Total	0.0000	20					
Δ_{Mo}	Model	0.0237	9	0.0009	1.11	0.0470	0.70	Significant
	Linear	0.0782	3	0.0008	0.9690	0.4419		
	$CaO.TiO_2$	0.0752	1	4.260E-07	0.0005	0.9825		
	$CaO.SiO_2$	0.0423	1	0.0024	2.89	0.1174		
	$CaO.Al_2O_3$	0.0482	1	0.0020	2.36	0.1525		
	$TiO_2.SiO_2$	0.8230	1	0.0009	1.04	0.3304		
	$TiO_2.Al_2O_3$		1	0.0033	3.91	0.0736		
	$SiO_2.Al_2O_3$		1	0.0026	3.05	0.1088		
	Residual	0.0752	11	0.082				
	Total	0.0178	20					
Δ_{Ni}	Model	0.0018	9	0.0002	1.36	0.0456	0.72	Significant
	Linear	0.0004	3	0.0001	0.8237	0.5077		
	$CaO.TiO_2$	2.094E-07	1	2.094E-07	0.0014	0.9703		
	$CaO.SiO_2$	0.0002	1	0.0002	1.05	0.3280		
	$CaO.Al_2O_3$	0.0003	1	0.0003	1.98	0.1868		
	$TiO_2.SiO_2$	0.0003	1	0.0003	2.06	0.1792		
	$TiO_2.Al_2O_3$	0.0000	1	0.0000	0.2240	0.6453		
	$SiO_2.Al_2O_3$	0.0001	1	0.0001	0.4565	0.5132		
	Residual	0.0016	11	0.0001				
	Total	0.0034	20					
Δ_{Cr}	Model	0.0005	13	0.0000	3.81	0.0417	0.75	Significant
	Linear	0.0001	3	0.0000	1.80	0.2355		
	$CaO.TiO_2$	0.0000	1	0.0000	2.19	0.1824		
	$CaO.SiO_2$	2.417E-06	1	2.417E-06	0.2315	0.6451		
	$CaO.Al_2O_3$	3.709E-08	1	3.709E-08	0.0036	0.9541		
	$TiO_2.SiO_2$	0.0000	1	0.0000	1.15	0.3187		
	$TiO_2.Al_2O_3$	2.510E-06	1	2.510E-06	0.2404	0.6389		
	$SiO_2.Al_2O_3$	3.064E-06	1	3.064E-06	0.2935	0.6048		
	$CaO.TiO_2.SiO_2$	0.0001	1	0.0001	5.92	0.0452		
	$CaO.TiO_2.Al_2O_3$	0.0001	1	0.0001	5.09	0.0586		
	$TiO_2.SiO_2.Al_2O_3$	0.0000	1	0.0000	1.47	0.2645		
	$TiO_2.SiO_2.Al_2O_3$	9.154E-07	1	9.154E-07	0.0877			
	Residual	0.0001	7	0.0000				
	Total	0.0006	20					

carbon into its oxides during slag-metal interactions becaue in high temperature region flux ingreditents such as CaO, SiO_2 and Al_2O_3 decomposed to release the free oxygen ions. These free oxygen ions (O^-) react with the carbon ions from the parent as well as filler metal and forming its oxides [22, 24–26]. Fron Table 3 it has been noticed that weld bead silicon content for all the twenty one experiments have been significantly increased as compared to base metal silicon content. From Eq. 5 it has been observed that individual flux ingredient TiO_2 and SiO_2 increases the weld bead silicon content and shows synergistic effect on Δ_{Si} while CaO and Al_2O_3 shows opposite effect on Δ_{Si}. Binary mixture interaction $CaO.TiO_2$ and $TiO_2.SiO_2$ gives negative effect on Δ_{Si} and decreases its content in weld region while $CaO.SiO_2$,

$CaO.Al_2O_3$, $TiO_2.Al_2O_3$ and $SiO_2.Al_2O_3$ binary interactions gives positive effect on Δ_{Si} content. The negative effect of individual flux ingredients on Δ_{Si} content may be due to the formation of silicates or other complex compounds which was cross checked by XRD and FTIR analysis of the flux specimen as shown in Fig. 3a-b. The incease of Δ_{Si} in the weld bead may be due to the presence of SiO_2 in the flux which dissociates in free silicon and oxygen ions in weld pool region. CaO has insignificant role in increasing the weld bead Δ_{Si} content because calcium oxide dissociates to Ca^{++} ions and free oxygen ions which in turns react with free silicon ions present in the arc region and forms SiO_2 and calcium react with oxygen and again form CaO [27, 28]. From Table 4 it has been observed that Δ_{Mn} value for all the experiments decreased. Individual flux ingredient TiO_2 and Al_2O_3 shows negative effect on Δ_{Mn} content while CaO and SiO_2 gives positive

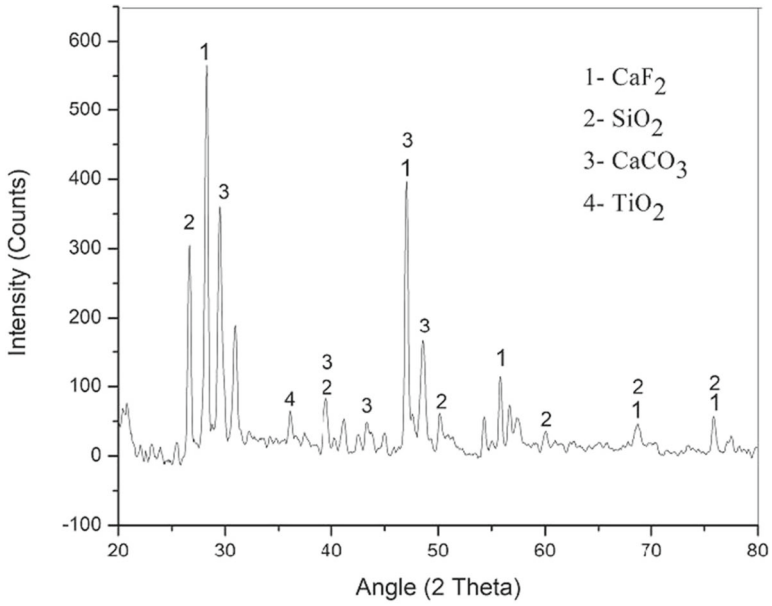

(a) XRD plot

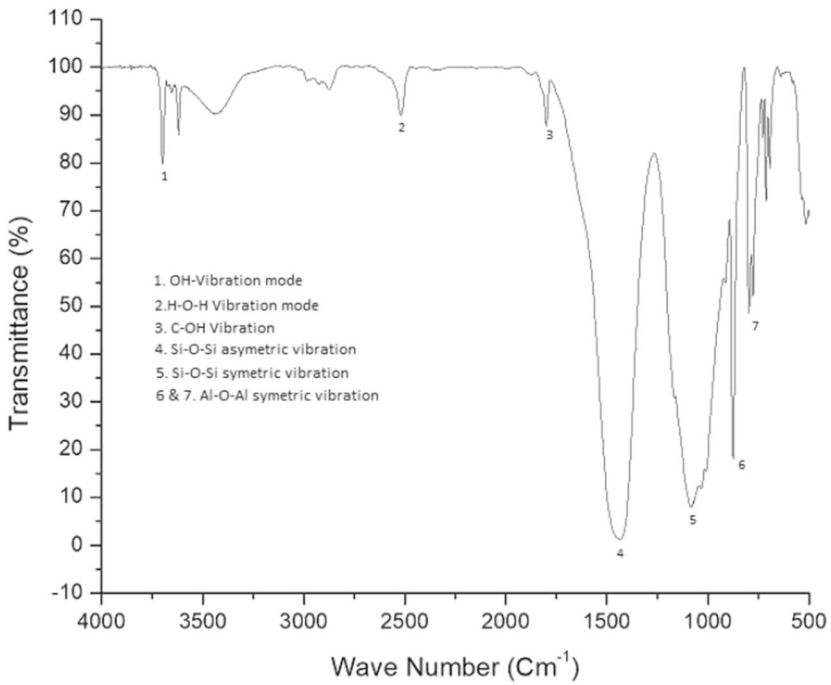

(b) FTIR plot

Fig. 3 **a** XRD plot of slag 6; **b** FTIR plot of slag 6

effect on Δ_{Mn} content. Binary interactions $CaO.TiO_2$, $CaO.SiO_2$, $CaO.Al_2O_3$ and $TiO_2.SiO_2$ gives antisynergistic effect on Δ_{Mn} and decreases its weld metal manganese content while $TiO_2.Al_2O_3$ and $SiO_2.Al_2O_3$ interactions gives positive effect on it (Eq. 6). Previous literature suggests that transfer of manganese basically depends upon the flux and filler wire composition [29, 30]. All the individual flux elements shows synergistic effect on Δ_P content and increases weld bead phosphorous content while TiO_2 is the only flux element which reduces its content in weld region. All the binary mixture interactions gives antisynergistic effect on Δ_P while all the ternary mixture shows positive effect on Δ_P and increases its content in weld region (Eq. 7). Ternary interactions shows more dominating effect as compared to the primary and secondary mixture interactions due to this reason Δ_P content increased in weld region. From Table 4 it has been observed that there was significant reduction in the weld metal sulphur content as compared to the base metal. Only flux f_8, f_{16}, f_{18} and f_{20} increases the Δ_S content in weld region. From regression Eq. 8 it has been noticed that all the primary flux ingredients shows negative effect on Δ_S and significantly reduces its content in weld region while all the binary mixture interactions gives opposite effect on Δ_S content. Available literature suggests that weld impurities are well addressed by lime fluxes, because when calcium oxide reacts with sulphur it forms calcium sulphide (CaS) and free oxygen by lowering the sulphur content in the weld region [31]. From Table 4 it has been observed that weld metal molybdenum (Δ_{Mo}) content significantly increased from the parent metal content. Primary flux ingredient CaO and SiO_2 shows negative effect on Δ_{Mo} and tends to reduce its content in weld region while TiO_2 and Al_2O_3 gives opposite effect on Δ_{Mo} content. Most of the binary interactions decreases the Δ_{Mo} content except $CaO.TiO_2$ and $CaO.SiO_2$ which shows positive effect on it. From Table 4 it has been observed that Δ_{Ni} content for all the experiments decreased. Primary flux ingredents CaO and Al_2O_3 shows antisynergistic effect on Δ_{Ni} and thus decrease its effect while SiO_2 and TiO_2 increases weld metal nickel content due its synergistic effect. All the binary interactions increases weld metal nickel content due to its synergistic effect on Δ_{Ni} while $CaO.SiO_2$ and $TiO_2.SiO_2$ gives antisynergistic effect (Eq. 10). Weld metal Δ_{Cr} content has been increased significantly for all the experiments (Table 4). CaO and TiO_2 primary flux ingredient decreases the Δ_{Cr} content while SiO_2 and Al_2O_3 shows positive effect on Δ_{Cr} and increases its value in weld region. Binary interactions $CaO.SiO_2$, $CaO.Al_2O_3$ and $SiO_2.Al_2O_3$ shows antisynergistic effect on weld metal chromium content and thus decreases Δ_{Cr} value while $CaO.TiO_2$, $TiO_2.SiO_2$ and $TiO_2.Al_2O_3$ interactions shows positive effect on Δ_{Cr} value. Antisynergistic effect was observed with ternary interactions $CaO.TiO_2.SiO_2$, $CaO.TiO_2.Al_2O_3$ and $TiO_2.SiO_2.Al_2O_3$ and thus reduces the weld metal Δ_{Cr} value while $CaO.SiO_2.Al_2O_3$ interaction gives positive effect and increases its value in weld region. Chromium is a strong carbide forming element and is also responsible for reducing the corrosion behaviour of low alloys steels. CaO and SiO_2 from flux react with chromium present in base and filler metal and will form chromium oxide and free oxygen and fluorine. Free oxygen again re-react with the calcium ions (Ca^{++}) and silicon ions present in the molten pool to form CaO and SiO_2 [32–34].

3.3 XRD and FTIR Analysis

After bead on plate experimentation, XRD and FTIR analysis of flux number five was carried out to verify the different phase phases and their bonding intertion present in the slag. By varying the 2θ difraction angle mode from 10° to 90° slag sample 5 was analyzed. Figure 3a shows the slag analysis of sample 6 which verify various crystaline phases were observed and in close agreemnt with the previous literature [14, 15]. Figure 3b shows the FTIR analysis of slag sample 5 which was performed in the range of 400–4000 cm^{-1} wavenumber at a resolution of 2 cm^{-1}. Different peaks were observed at different wavenumbers. OH-vibration streching mode was noticed at a peak near around 800 cm^{-1} and Ti-O streching mode was observed between 1000 and 1100 cm^{-1} while Si-O asymetric mode was seen at 1500 cm^{-1}. Small peaks of hydroxyl group near abut 3000–3200 cm^{-1} was noticed and are in close arrement with the previous literature [9, 10].

3.4 Microstructure Analysis

Microstructure of some of the weld beads were analysed to verify the presence of carbide inclusions using optical microscope. API X70 weld metal basically exhibit acicular ferrite microstructure with some inclusions of carbides dispersed in it [35, 36]. From Table 4 it has been noticed that carbon content in the weld bead significantly increased which is verified from the micrographs shown in Fig. 4.

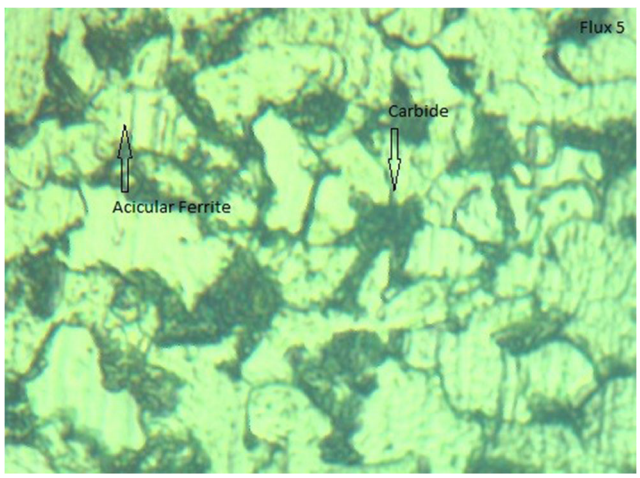

Fig. 4 Microstructure of weld bead for flux 5

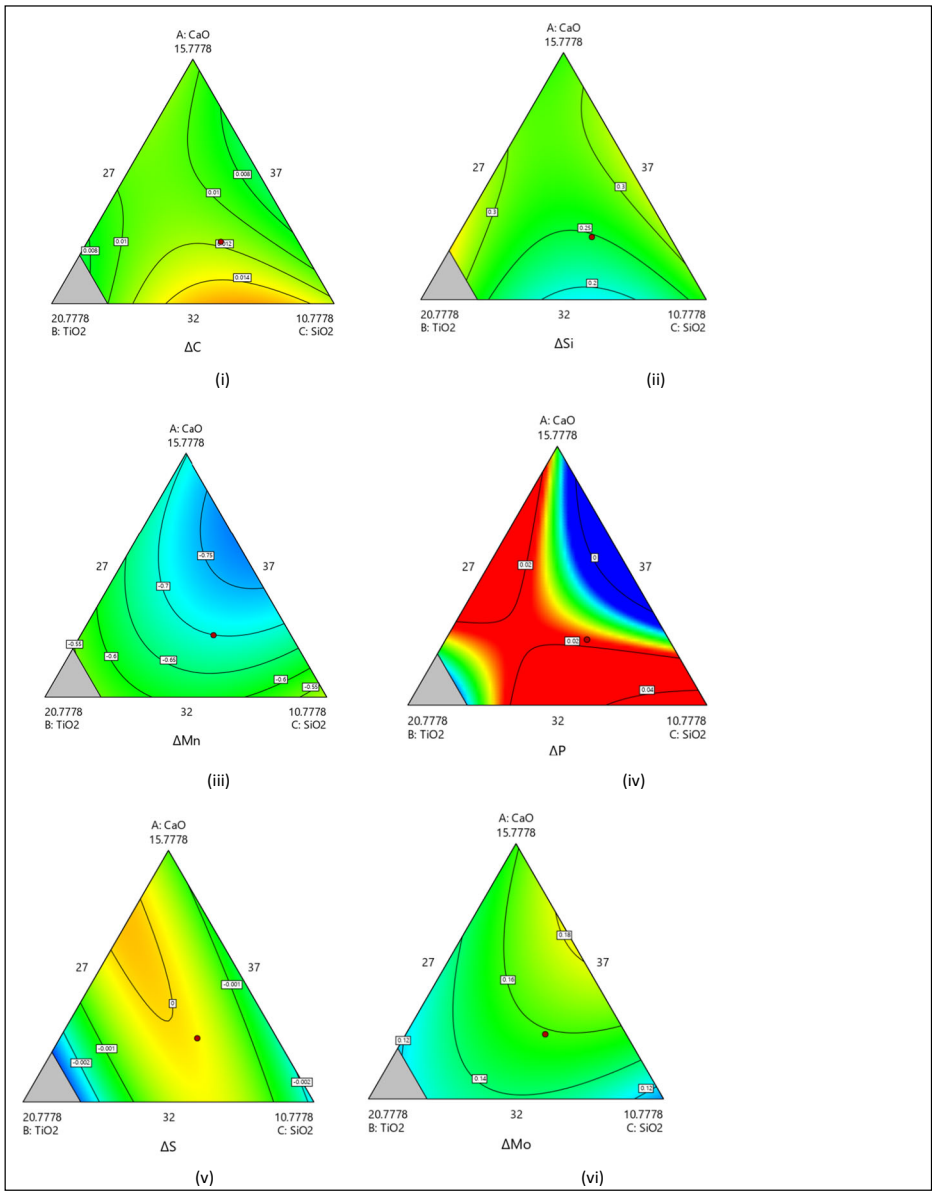

Fig. 5 **a-b** Curves for different Δ transfer responses

Table 6 Desired values of different Δ responses

S.No	CaO	TiO_2	SiO_2	Al_2O_3	Δ_C	Δ_{Si}	Δ_{Mn}	Δ_P	Δ_S	Δ_{Mo}	Δ_{Ni}	Δ_{Cr}	Desirability
1	32.0	30.0	20.9	7.0	0.0116	0.17255	−0.36525	0.01575	−0.0004	0.18365	−0.182	0.0443	0.80
2	20.1	34.3	23.5	12	0.00498	0.14336	−0.67672	0.00604	−0.00202	0.1681	−0.18842	0.04348	0.91
3	30.1	24.0	27.0	8.8	0.00504	0.33498	−0.51466	0.00622	−0.00256	0.1228	−0.15546	0.04324	0.82

Table 7 % error values for Δ_C, Δ_{Si}, Δ_{Mn} & Δ_P responses

Flux Components				PV				AV				E			
CaO	TiO_2	SiO_2	Al_2O_3	Δ_C	Δ_{Si}	Δ_{Mn}	Δ_P	Δ_C	Δ_{Si}	Δ_{Mn}	Δ_P	Δ_C	Δ_{Si}	Δ_{Mn}	Δ_P
32.0	30.0	20.9	7.0	0.0119	0.17133	−0.36450	0.01580	0.0116	0.17255	−0.36525	0.01575	0.98	0.82	0.63	0.98
20.1	34.3	23.5	12	0.00502	0.14333	−0.68555	0.00610	0.00498	0.14336	−0.67672	0.00604	0.99	0.61	0.48	1.03
30.1	24.0	27.0	8.8	0.00508	0.33500	−51,470	0.00625	0.00504	0.33498	−0.51466	0.00622	0.99	0.70	0.82	0.88

3.5 Contour Curves for Different Responses

Variation in change in Δ element has been observed on the different regions on contour curves. Variation in the element transfer can be observed on the surface of the contour curve which gives the constant value of Δ while flux mixture combination was well seen by dotted points on the curves [34]. Curves indicating the predicted values for different responses such as Δ_C, Δ_{Si}, Δ_{Mn}, Δ_P, Δ_S, Δ_{Mo}, Δ_{Ni} and Δ_{Cr} are shown in Fig. 5a-b.

3.6 Optimization & Validation of Model

To optimize the Δ quantities of weld beads similar to the base metal an attempt has been made. To simultaneously optimize all the responses a compound desirability optimization technique used which was given by derringer and suich [37]. Table 6 represents the desirability values of different Δ quantities. To find the error (E) values of different Δ responses, 3 flux compositions with larger desirability value was chosen for the study [38]. Table 7 represents percentage error values for different Δ responses.

4 Conclusion

- Weld bead carbon content for all the experiments has been increased while it is lower than that of base metal. Individual flux ingredients CaO and SiO_2, has synergistic effect on Δ_C and increases its weld bead carbon content while TiO_2 and Al_2O_3 shows antisynergistic effect on Δ_C and decreases the delta carbon content in weld region. All the binary mixture interactions gives synergistic effect on Δ_C and increases its weld metal carbon content except $CaO.SiO_2$ interaction which decreases its weld metal carbon.
- Weld bead Δ_{Si} content for all the twenty one experiments have been significantly increased as compared to base metal silicon content. Primary flux ingredient TiO_2 and SiO_2 increases the weld bead silicon content and shows synergistic effect on Δ_{Si} while CaO and Al_2O_3 shows opposite effect on Δ_{Si}.
- Binary interactions $CaO.TiO_2$, $CaO.SiO_2$, $CaO.Al_2O_3$ and $TiO_2.SiO_2$ gives antisynergistic effect on Δ_{Mn} and decreases its weld metal manganese content while $TiO_2.Al_2O_3$ and $SiO_2.Al_2O_3$ interactions gives positive effect on it.
- All the primary flux elements shows synergistic effect on Δ_P content and increases weld bead phosphorous content. Reduction in the weld metal sulphur content was observed as compared to the base metal while flux f_8, f_{16}, f_{18} and f_{20} increases the Δ_S content in weld region.
- There is significant increase in weld metal molybdenum (Δ_{Mo}) content as compared to the parent metal content. Primary flux elements CaO and SiO_2 gives antisynergistic effect while TiO_2 and Al_2O_3 provide synergistic effect on Δ_{Mo} content.
- Weld metal Δ_{Cr} content has been increased significantly for all the experiments as compared to base metal.

Acknowledgements It is requested to editorial board to please acknowledge the present research for possible publication in Silicon journal. The content is new and unpublished.

Authors' Contributions It is certified on behalf of corresponding author (Lochan Sharma) that all authors are equally contributed in the present manuscript.

Data Availability I Lochan Sharma (Corresponding Author) certified that data & material will be available on author's request.

Declarations

Ethical Approval I Lochan Sharma (Corresponding Author) on behalf of other co-authors certified that I have taken the ethical approval to publish the data presented in the manuscript. Also the data used in this manuscript (such as figures) has been cited in this paper.

Consent to Participate NA.

Consent of Publication I Lochan Sharma (Corresponding Author) on behalf of other coauthors certified that I have taken the permission to publish the present content.

Competing Interests It is certified on behalf of corresponding author (Lochan Sharma) that present research is not funded by any external agency and authors declared that there is no conflicts of interest in the present research.

Conflicts of Interests It is certified on behalf of corresponding author (Lochan Sharma) that present research is not funded by any external agency and authors declared that there is no conflicts of interest in the present research.

Research Involving Human Participants and/or Animals The present research is involved for human participants.

Informed Consent NA.

References

1. Grey JM (2002) An independent view of linepipe and linepipe steel for high strength pipelines. Microalloying international, LP, Houston, Texas, X80 pipeline cost workshop
2. Liu C, Bhole SD (2013) Challenges and developments in pipeline weldability and mechanical properties. Sci Technol Weld Join 18(2):169–181
3. Das AK (2010) The present and the future of line pipe steels for petroleum industry. Mater Manuf Process 25:14–19
4. Hillenbrand HG, Kalwa C (2002) High strength line pipe for project cost reduction. World Pipelines 2:1–10
5. Chai CS, Eagar TW (1981) Slag-metal equilibrium during submerged arc welding. Metall Trans B 12:53–47
6. Mitra U, Eagar TW (1991) Slag-metal reactions during welding: part I. Evaluation and reassessment of existing theories. Metall Trans B 22:65–71
7. Dallam CB, Liu S, Olson DL (1985) Flux composition dependence of microstructure and toughness of submerged arc HSLA weldments. Weld J 64:52
8. Paniagua-Mercado AM, Lopez-Hirata VM, Saucedo Munoz ML (2005) Influence of the chemical composition of flux on the microstructure and tensile properties of submerged-arc welds. J Mater Proc Technol 169:34–51
9. Shu Q, Wang Y, Li J, Chou CK (2015) Effect of Na_2O on dissolution rate of alumina in CaO-Al2O3-MgO-SiO2 slag. ISIJ Int 55(11):2297–2303
10. Sharma L, Chhibber R (2019) Investigating the physicochemical and thermophysical properties of submerged arc welding fluxes designed using TiO2-SiO2-MgO and SiO2-MgO-Al2O3 flux systems for linepipe steels. Ceram Int 45:1569–1587
11. Tuliani SS, Boniszewski T, Eaton NF (1969) Notch toughness of commercial submerged arc weld metal. Weld Met Fabr 37:32–39
12. Eagar TW (1978) Sources of weld metal oxygen contamination during submerged arc welding. Weld J 57:76
13. Coetsee T, Mostert RJ, Pistorius PGH (2021) The effect of flux chemistry on element transfer in submerged arc welding: application of thermochemical modelling. J Mater Res Technol 11:2021–2036
14. Jindal S, Chhibber R, Mehta NP (2015) Prediction of element transfer due to flux and optimization of chemical composition and mechanical properties in high-strength low-alloy steel weld. Proc Inst Mech Eng B J Eng Manuf 229:785–801
15. Kanjilal P, Pal TK, Majumdar SK (2006) Combined effect of flux and welding parameters on chemical composition and mechanical properties of submerged arc weld metal. J Mater Process Technol 171:223–231
16. Kanjilal P, Pal TK, Majumdar SK (2007) Prediction of element transfer in submerged arc welding. Magnesium 10:40
17. Burck PA, Indacochea JE, Olson DL (1990) Effects of welding flux additions on 4340 steel weld metal composition. Weld J 3:115–122
18. Beidokhti B, Koukabi AH, Dolati A (2009) Influences of titanium and manganese on high strength low alloy SAW weld metal properties. Mat Charact 6:225–233
19. Trindade BV, Payao CD, Souza J, Paranhos GFL (2007) The role of addition of Ni on the microstructure and the mechanical behaviour of C-Mn weld metals. Exacta 5:177–183
20. Yoshino Y, Stot RD (1979) Effect of microalloys on the notch toughness of line pipe seam welds. Weld Res Suppl 1:2–5
21. Cornell JA (2011) Experiments with mixtures: designs, models, and the analysis of mixture data. Wiley, New York
22. Eriksson G, Pelton AD (1993) Critical evaluation and optimization of thermodynamic properties and phase diagrams of the CaO-Al_2O_3, Al_2O_3-SiO_2 and CaO- SiO_2-Al_2O_3 systems. Metall Mater Trans B 24:807–816
23. Anderson VL, McLean RA (1974) Design of experiments: a realistic approach. Marcel Dekker, Inc., New York
24. Kanjilal P, Majumdar SK, Pal TK (2005) Prediction of acicular ferrite from flux ingredients in submerged arc weld metal of C-Mn steel. ISIJ Int 45:876–885
25. Pandey ND, Bharti A, Gupta SR (1994) Effect of submerged arc welding parameters and fluxes on element transfer behaviour and weld-metal chemistry. J Mater Process Tech 40:195–211
26. Kanjilal P, Pal TK, Majumdar SK (2007) Prediction of element transfer in submerged arc welding. Weld J 86:135s–146s
27. Chang KL, Huang CT, Huang W et al (2008) Investigations of microstructure and phosphorus distribution in BOF slag. China Steel Tech Rep 21:1–6
28. Bhandari D, Chhibber R, Arora N (2012) Effect of electrode coatings on diffusible hydrogen content, hardness and microstructures of the ferritic heat affected zones in bimetallic welds. Adv Mater Res 383:4697–4701
29. Singh K, Pandey S (2008) Economics of recycling submerged arc welding slag as a flux. In: Proceedings of the 8th international conference on trends in welding research, Pine Mountain, GA, Materials Park, OH: ASM International, 2, pp 806–810
30. Jindal S, Chhibber R, Mehta NP (2014) Effect of welding parameters on bead profile, microhardness and H2 content in submerged arc welding of high-strength low-alloy steel. Proc Inst Mech Eng B J Eng Manuf 228:82–94
31. Paniagua-Mercado AM, Lopez-Hirata VM (2011) Chemical and physical properties of fluxes for SAW of low-carbon steels. Arc Welding 13:281–298
32. Plessis Du J, du Toit M, Pistorius PC (2007) Control of diffusible weld metal hydrogen through flux chemistry modification. Weld J 86:273s–280s
33. Ramirez JE (2008) Characterization of high-strength steel weld metals: chemical composition, microstructure, and non-metallic inclusions. Weld J 87:65s–75s

34. Hummel FA (1984) Introduction to phase equilibrium in ceramics systems. CRC Press Ltd, Boca Raton
35. Waris KN, Rahul C (2021) Experimental investigation on dissimilar weld between super duplex stainless steel 2507 and API X70 pipeline steel. Proc Inst Mech Eng L J Mater Des Appl 235(8): 1827–1840. https://doi.org/10.1177/14644207211013056
36. Waris KN, Rahul C (2021) Characterization of CaO-CaF2-TiO2-SiO2 based welding slags for physicochemical and thermophysical properties. Silicon 13(7):1575–1589. https://doi.org/10.1007/s12633-020-00537-8
37. Derringer G, Suich R (1980) Simultaneous optimization of several response variables. J Qual Technol 12:214–219
38. Harrington EC (1965) The desirability function. Ind Qual Control 21:494–498